PIV of the flow over a NREL S826 airfoil subjected to different ice accretions

Magnus K. Vinnes, Leon Li and R. Jason Hearst

DOI: https://doi.org/10.1007/978-3-030-22196-6_52

Abstract The flow field over a NREL S826 airfoil subjected to different ice accretions has been investigated by particle image velocimetry for angles of attack ranging from -4° to 16°. The results have been compared to previously acquired force measurements. For streamlined ice accretions, increased surface roughness and changes to the combined airfoil-ice geometry lead to reduced aerodynamical performance of the airfoil. However, the streamlined ice accretions might act as leading edge flaps at high angles of attack, delaying stall. For the horn ice accretion, a large separation bubble occurs behind the horn reducing the performance of the airfoil, and initiating stall at a lower angle of attack compared to the other cases.

1 Introduction

Wind turbines in cold climates are subjected to icing atmospheric conditions. Ice accretion on the turbine blades leads to reduced performance of the turbine. Han et al. [7] found that a turbine subjected to icing required 70% more torque to keep the same rotational velocity as a clean turbine. A full scale test turbine, at the Acqua Spruzza test site in Italy, experienced a reduction of 19% in power production when subjected to icing [2].

Ice accretions on airfoils are usually named by the atmospheric icing conditions in which they developed, that is, glaze, rime or mixed icing. However, Bragg et al. [3] state that it is more meaningful to define ice accretions by their geometry when the aerodynamics and performance of the airfoil are investigated.

Magnus K. Vinnes
Norwegian Univ. of Science and Technology, Trondheim, Norway e-mail: magnus.kyrkjebo@ntnu.no

Leon Li
Norwegian Univ. of Science and Technology, Trondheim, Norway e-mail: leon.li@ntnu.no

R. Jason Hearst
Norwegian Univ. of Science and Technology, Trondheim, Norway e-mail: jason.hearst@ntnu.no

They separate ice geometries into roughness icing, horn icing, streamwise icing and streamwise-ridge icing [1].

Several studies have measured the forces acting on airfoils subjected to icing [6, 8, 13]. The airfoils generally experience reduced lift and increased drag. The magnitude of these changes vary due to the different airfoils used, as well as the icing geometries, icing roughness, wind speeds, and angles of attack (AoA). Earlier works performed on the aerodynamics of iced airfoils are limited to symmetrical airfoils, or airfoils intended for aircraft. They focus on a limited range of AoA, and only look into one ice accretion (e.g. [5, 10, 11, 14]). This study focuses on the flow field over a NREL S826 airfoil intended for medium-sized wind turbines. Experiments were performed on AoAs ranging from -4° to 16°, for the clean configuration and three different ice accretions.

2 Experimental set-up

PIV experiments were conducted in the closed-loop wind tunnel at NTNU, with test section dimensions of 12 m $\times$ 1.8 m $\times$ 2.7 m (length $\times$ height $\times$ width). Figure 1 shows the experimental set-up, seen from the test section inlet.

The airfoil used in the experiments was a NREL S826 airfoil with a chord length of $c = 0.45$ m. Three different 3D-printed ice geometries, shown in Fig 2, were attached to the leading edge. They represent streamlined and horn icing geometries, but are here referred to by the atmospheric icing conditions they were generated in. The geometries were developed by Hann [9] with the LEWICE icing simulation software[2]. All experiments were performed with a chord based Reynolds number of $Re_c = U_\infty c/\nu = 4.5 \times 10^5$.

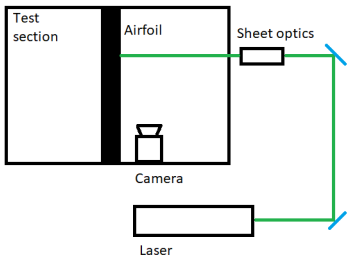

Fig. 1 Schematic of the front view of the experimental set-up. The airfoil and the camera were mounted to a force balance, allowing for the simultaneous rotation of both, ensuring the field of view was kept the same for all cases. To minimise distortion of the flow, the laser and the sheet optics were mounted outside the wind tunnel. Note that the schematic is not to scale.

[1] Please refer to reference [3] for further information about different icing geometries.

[2] Please refer to reference [9] for further information about the ice accretions and the atmospheric conditions they were developed in.

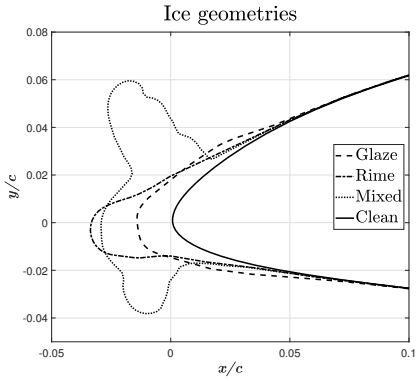

Fig. 2 Icing geometries developed by Hann [9] using LEWICE. Rime and glaze ice accretions have a streamlined shape, while the mixed icing has a horn geometry. The roughness height on the surface of the ice geometries was 0.6 mm for the glaze accretion and 1.0 mm for the rime and the mixed accretion. Roughness here is specifically used to describe the surface finish of the modelled icing geometry, not the geometry itself.

3 Results

Krøgenes and Brandrud [13] performed force measurements with the same experimental set-up. The lift coefficients obtained in their experiments are shown in Fig. 3, and the results in the present work are compared with their results. Note that the results were obtained at a slightly lower Reynolds number, $Re_c = 4.0 \times 10^5$. However, they found that aerodynamic performance has low dependency on Reynolds number above $Re_c = 2.0 \times 10^5$, which makes this a fair comparison.

The mean flow fields for all experimental cases are shown in Fig. 4. For the streamlined ice accretions, glaze and rime, no separation is visible for AoAs between -4° and 10°. This indicates that the reduced performances are due to increased surface roughness on the ice accretions compared to that on the clean airfoil, and changes in the ice accretions make to the airfoil geometry. Both streamlined accretions experience high lift at 14° AoA. Fig. 3 shows that there is a bump in the lift curve for the glaze accretion, while the linear lift region is extended for the rime icing. This is surprising, as the flow field observed in Fig. 4 differs between the iced

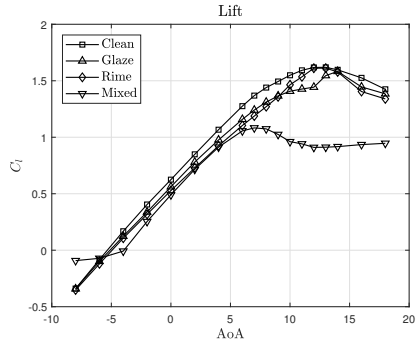

Fig. 3 Lift coefficient of the NREL S826 airfoil at different AoA and with the different ice accretions attached. A decrease in lift is observed when any of the ice accretions are present on the leading edge. The mixed accretion reduces stall AoA with approximately 5°.

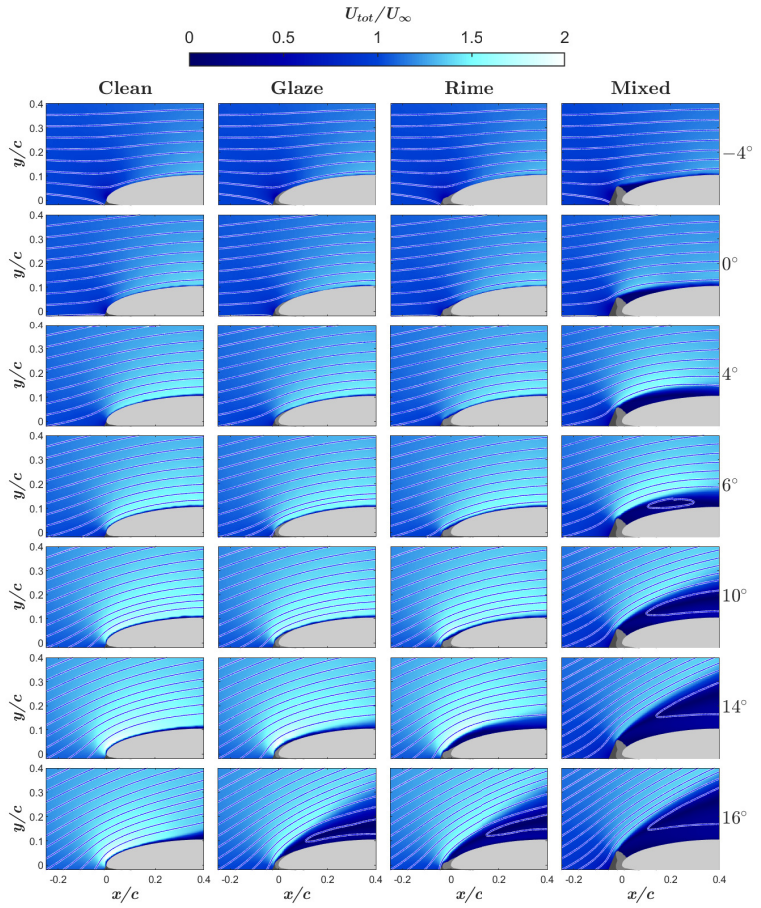

Fig. 4 Mean velocity field for all experimental cases. The velocity has been normalised by the freestream velocity. Different ice accretions are separated in columns, while different AoAs are separated by row.

cases and the clean airfoil for this AoA. One possible reason for this is discussed in the end of this section.

Looking at the mixed ice accretion, which has a horn like geometry, a separation bubble is observed behind the horn for all AoAs. The bubble increases in height and length with increasing AoA. The reduced performance of the airfoil, within the linear lift region, is therefore explained as an effect of the separation bubble. At an AoA around 7°, the flow is not able to reattach, which leads to the low stall angle.

The turbulent kinetic energy (TKE) was calculated as a two dimensional surrogate, $k_{2D} = \frac{1}{2}\left[\langle u^2\rangle + \langle v^2\rangle\right]$ and normalised by the square of the freestream velocity, U_∞^2. u and v are the fluctuating velocity components. The results for the four highest investigated AoAs are shown in Fig. 5.

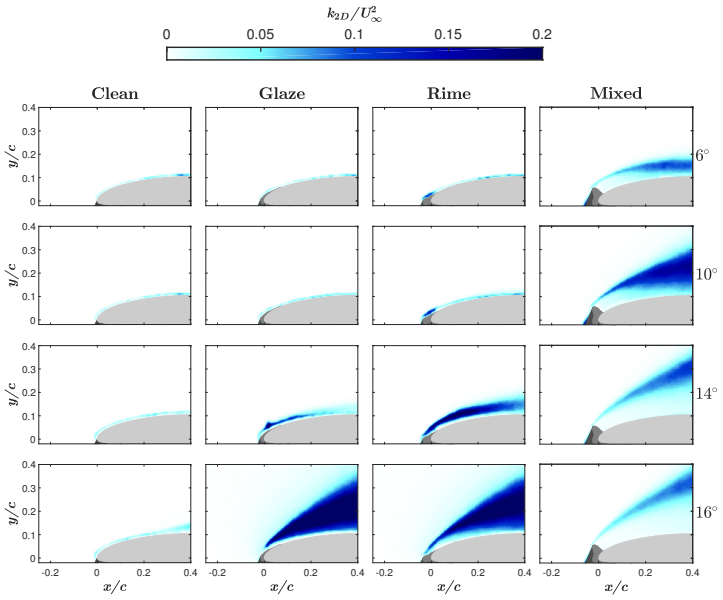

Fig. 5 Turbulent kinetic energy for all icing geometries, for the four highest AoA investigated, normalised by the square of the freestream velocity. Different ice accretions are separated in columns, while different AoAs are separated by row.

For the mixed accretion, high levels of TKE are found in the shear layer between the recirculating flow and the freestream flow. At 6° AoA there is a wide region of TKE close to the airfoil surface. This indicates that the shear layer is fluctuating, which in turn also causes the reattachment point to fluctuate. The region of high TKE close to the horn of the icing is much thinner. These observations agree with results obtained by Jacobs and Bragg [10, 11]. For the glaze and rime icings, some TKE is visible above the ice accretions, and to some extent also over the airfoil. This indicates that the flow separates. However, the region is thin compared to the completely stalled cases. This happens at AoAs where the airfoil experiences comparable lift between the streamlined icings and the clean case.

A possible reason for the high lift found for the glaze and the rime accretions at 14° AoA is that the icing acts as a leading edge flap. This has been suggested earlier by Jasinski et al. [12]. If the icing acts as a flap, an increase in the effective AoA would be expected. The effective AoA was calculated as the angle between the chord line and the mean flow direction at a distance $0.2c$ upstream of the leading edge. The results show a small increase for the glaze accretion and a larger increase for the rime accretion. This suggests that the rime icing may act as a leading edge flap. There is also a possibility that the glaze accretion does the same. However, this is only suggestive, as the increase in effective AoA could come from separation of the flow only.

4 Conclusion

The flow fields over an NREL S826 airfoil with three different ice accretions have been measured using PIV. A wide range of AoAs were investigated. The results show that for streamlined ice accretions, reduced performance is due to the roughness on the ice accretions and changes to the airfoil geometry. The maintenance of lift at high AoAs for the streamlined cases suggest they may act as a leading edge flaps. For horn ice accretions, the reduced performance is a result of the separation bubble behind the horn of the ice geometry.

References

1. Ansell PJ, Bragg MB (2014) measurement of unsteady flow reattachment on an airfoil with an ice shape. AIAA J 52:656–561
2. Botta G, Cavaliere M, Hottinen H (1998) Ice accretion at Acqua Spruzza and its effects on wind turbine operation and loss of energy. In Proc BOREAS IV
3. Bragg MB, Broeren AP, Blumenthal LA (2005) Iced-airfoil aerodynamics. Prog Aerosp Sci 41:323–362
4. Bragg MB, Broeren AP, Addy H et al (2007) Airfoil ice-accretion aerodynamic simulation. In Proc 45th AIAA Aerosp Sci Meet Exhib
5. DeGregorio F, Ragni A, Airoldi A et al (2001) PIV investigation on airfoil with ice accretions and resulting performance degration. In Proc ICIASF 2001 rec, 19th Internat Cong Instrum Aerosp Simul Facil 94–105
6. Etemaddar M, Hansen MOL, Moan T (2014) Wind turbine aerodynamic response under atmospheric icing conditions. Wind Energy 17:241–265
7. Han Y, Palacios M, Schmitz S (2012) Scaled ice accretion experiments on a rotating wind turbine blade. J Wind Eng and Ind Aerodyn 109:55–67
8. Han Y, Palacios J (2013) Airfoil-performance-degradation based on nondimensional icing parameters. AIAA J 51:2570–2581
9. Hann R (2018) UAV Icing: Comparison of LEWICE and FENSAP-ICE for ice accretion and performance degration. In Proc Atmos Space Environm Conf AIAA Aviat Forum
10. Jacobs JJ, Bragg MB (2006) Particle image velocimetry measurements of the separation bubble on an iced airfoil. In Proc 24th AIAA Appl Aerodyn Conf
11. Jacobs JJ, Bragg MB (2007) Two- and three-dimensional iced airfoil separation bubble on an iced airfoil. In 45th AIAA Aerosp Sci Meet Exhib
12. Jasinski W, Noe S, Selig MS et al. (1998) Wind turbine performance under icing conditions. J of Sol Eng 120:60–65
13. Krøgenes J, Brandrud L (2017) Aerodynamics performance of the NREL S826 Airfoil in icing conditions (Master's Thesis). NTNU, Trondheim
14. Mirzaei M, Ardekani MA, Doosttalab (2009) Numerical and experimental study of flow field characteristics of an iced airfoil. Aerosp Sci Tech 13:267–276
15. Parent O, Ilinca A (2011) Anti-icing and de-icing techniques for wind turbines: Critical review. Cold Reg Sci Tech 65:88–96